Vorticity Waves over Strong Topography

YVES GRATTON* AND PAUL H. LEBLOND

Department of Oceanography, The University of British Columbia, Vancouver, B.C., Canada V6T 1W5

(Manuscript received 27 November 1984, in final form 24 August 1985)

ABSTRACT

Analytical solutions are found for topographic waves propagating over steep bottom slopes in a two-layer infinite channel. From the inviscid unforced long-wave equation for a two-layer fluid on an *f*-plane, it is shown, under the assumption of a relatively thin upper layer, that barotropic waves force a baroclinic response through topographic coupling, resulting in surface intensified motion. Solutions are found with and without the small slope approximation. It is shown that the small slope approximation underestimates the frequency of low-frequency topographic waves, even when the slope is small. The theory is compared with observations from the Strait of Georgia and with a numerical model of the St. Lawrence estuary.

1. Introduction

The nature and origin of low-frequency subinertial motions observed in some semi-enclosed coastal basins, in particular the Strait of Georgia (Chang et al., 1976) and the St. Lawrence estuary (El-Sabh et al., 1982) continue to remain unexplained. Such motions account for up to 50% of the horizontal kinetic energy measured in those basins; they are characterized by their low-frequency (periods from 5–100 days) and short horizontal scale (a few km). The motions are also surface-intensified and appear uncorrelated with local wind or pressure systems. Attempts to describe their properties in terms of wave propagation have hitherto remained unsuccessful (Helbig and Mysak, 1976; Schott and Mysak, 1980), and it has been suggested that these motions might partake more of the nature of large scale turbulence than of wave motion, resulting perhaps from an energy cascade originating with fortnightly tidal forcing (LeBlond, 1983). Consideration of the wave theories shows, however, that they are mostly limited to gently sloping topographies; such a weak slope assumption is clearly invalid in the situations considered above as well as on many continental shelves. In this paper, we consider subinertial wave propagation in channels with steeply sloping topography, in the presence of rotation and stratification. Although the stratification will be approximated by a two-layer fluid, the results should be relevant to the low-frequency dynamics of the coastal basins mentioned above as well as to the theory of continental shelf waves.

This work extends earlier studies of vorticity wave propagation along sloping oceanic boundaries, arising from Robinson's (1964) first analysis of continental

* Present address: Depart. Océanographie, UQAR Rimouski, P.Q., Canada G5L 3A1.

shelf waves. Mysak (1980) has recently reviewed the subject. Of actual and theoretical coastal slope profiles considered, only the simplest (such as the exponential depth profile of Buchwald and Adams, 1968) allows solutions and dispersion relations to be expressed by analytical expressions. The combination of stratification and bottom relief gives rise to complications which are best understood for weakly sloping ocean models or linear beaches (see, for example, the review by Hendershott, 1981). Our interest focuses on steeply sloping bottoms. As in Allen (1975) we will work with a two-layer model. We will formulate the problem in terms of a pair of coupled partial differential equations, for the mass-transport stream function and interfacial displacement respectively but will not follow Allen's path in decoupling the equations. We do not assume that the offshore baroclinic scale (the internal Rossby radius of deformation) is much smaller than the topographic scale (the shelf width); our pair of equations remain coupled. The one fundamental approximation which we invoke to simplify the problem consists of assuming that the upper layer is relatively thin. The coupling is then only one-way: the barotropic motions force an interfacial oscillation which provides a surface-intensified structure to vorticity waves whose horizontal scales are those of barotropic modes. We thus discuss neither free interfacial modes nor Kelvin waves, which have already been thoroughly explored, but focus our attention on modes which are barotropic in their dynamics, but which produce significant interfacial motion via bathymetric coupling.

We define and formulate the problem in section 2, obtaining the pair of partial differential equations referred to before and the boundary and matching conditions which they must satisfy. The simplifying assumption of a thin upper layer is introduced and its consequences discussed in section 3. Solutions for channels of linear and parabolic profiles are obtained

in the following sections; the influence of slope steepness on the solutions and on the dispersion relation are also discussed. Applications to specific basins and channels are considered in section 7.

2. General formulation of the problem

In order to examine the coupling of interfacial motion to bottom slopes, we consider a two-layer model. The upper layer and lower layer densities ρ_1 and ρ_2 are near enough that

$$0 < j = (\rho_2 - \rho_1)/\rho_2 \ll 1.$$

The geometry of the problem is illustrated in Fig. 1a. The oceanic fluid has an equilibrium depth $H(x, y)$ divided in upper and lower layers of thickness $H_1(x, y)$ and $H_2(x, y)$ respectively; $H_1 + H_2 = H$. Since H_1, H_2 and H are generally varying, we shall use D_1, D_2, $D = D_1 + D_2$ as constant scale depths to represent typical values of H_1, H_2, H. Displacement of the ocean surface and interface from equilibrium levels are referred to as $\eta_1(x, y, t)$ and $\eta_2(x, y, t)$. Velocity components u, v in the x, y directions respectively bear subscripts 1 and 2 in the upper and lower layers. The motion in each layer is governed by the linearized momentum and volume continuity equations for an inviscid fluid on the f-plane (LeBlond and Mysak, 1978, p134). Thus,

$$u_{1_t} - fv_1 + g\eta_{1_x} = 0 \tag{1a}$$

$$v_{1_t} + fu_1 + g\eta_{1_y} = 0 \tag{1b}$$

$$(H_1u_1)_x + (H_1v_1)_y = (\eta_2 - \eta_1)_t \tag{1c}$$

$$u_{2_t} - fv_2 + g'(\eta_2 - \eta_1)_x + g\eta_{1_x} = 0 \tag{2a}$$

$$v_{2_t} + fu_2 + g'(\eta_2 - \eta_1)_y + g\eta_{1_y} = 0 \tag{2b}$$

$$(H_2u_2)_x + (H_2v_2)_y = -\eta_{2_t}. \tag{2c}$$

Differentiation with respect to time (t) and spatial coordinates (x, y) has been denoted by subscripts; $g' = gj$ is the reduced gravity. The mean upper thickness H_1 is assumed uniform in the present context. This system of equations has been applied to basins and channels by Gratton (1983); only channels with axis along the y-coordinate and lateral scale $2L$ are considered here. The channel geometry is shown in Fig. 1b. A long-channel scale for the motion shall be λ, a wavelength. For horizontal scales of motion short compared to the external Rossby radius $(gD)^{1/2}/f$, the upper surface $(z = \eta_1)$ may be considered rigid (Pedlosky, 1979). This approximation filters out surface waves. Neglecting η_{1_t} in (1c) allows the introduction of the mass-transport stream function ψ, related to the vertically integrated transport via
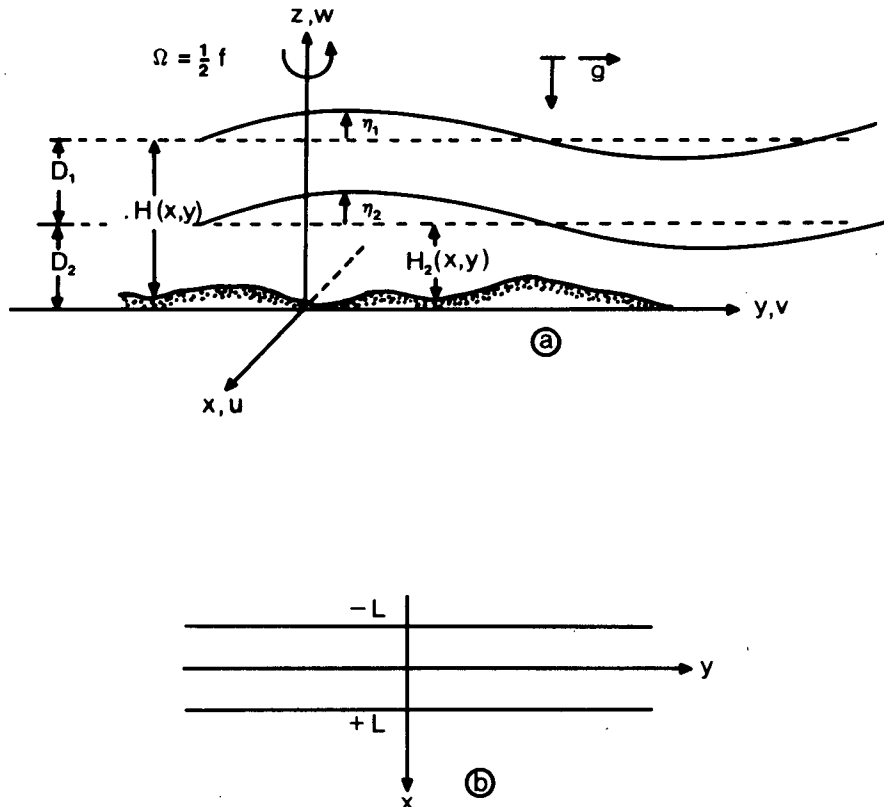

FIG. 1. Coordinate system and variables.

$$\psi_x = (H_1 v_1 + H_2 v_2), \tag{3a}$$

$$\psi_y = -(H_1 u_1 + H_2 u_2). \tag{3b}$$

Following Allen (1975), it is then possible to reduce the basic equations (1) and (2) to the coupled second-order system for ψ and $\eta = \eta_2$ (the subscript becomes superfluous):

$$(H\nabla^2\psi - H_x\psi_x - H_y\psi_y)_t + f(H_x\psi_y - H_y\psi_x)$$
$$= -g'H_1(H_y\eta_x - H_x\eta_y) \tag{4}$$

$$\left[H\nabla^2\eta - \frac{H_1}{H_2}(H_x\eta_x + H_y\eta_y) - \frac{H^2 M(\eta)}{g'H_1 H_2} \right]_t$$

$$+ \frac{fH_1}{H_2}(H_x\eta_y - H_y\eta_x) = \frac{-1}{g'H_2}[M(\psi_x)H_y - M(\psi_y)H_x]. \tag{5}$$

Here $M(*)$ stands for the differential operator $\partial_{tt}^2 + f^2$; $H_{x,y} = (H_1 + H_2)_{x,y} = H_{2_{x,y}}$. These equations are dimensional equivalents to Eqs. (2.17a, b) of Allen (1975). In the absence of bottom slopes the inhomogeneous terms coupling (4) and (5) vanish and the system (4)–(5) describes independent barotropic and baroclinic modes, characterized respectively by the variations in the transport stream function ψ and the interfacial displacement η. Although purely independent modes are no longer possible in the presence of bottom slopes we shall continue, for convenience, to refer to those components of the motion associated with ψ and η as barotropic and baroclinic respectively.

We now restrict our attention to low-frequency motions, for which $M \approx f^2$, in a channel oriented along the y-axis, in which $H_2 = H_2(x)$ only. The governing equations (4)–(5) reduce to

$$(H\nabla^2\psi - H_x\psi_x)_t + fH_x\psi_y = g'H_1 H_x\eta_y \tag{6}$$

$$\left[H\nabla^2\eta + \frac{H_1}{H_2}H_x\eta_x - \frac{H^2 f^2}{g'H_1 H_2}\eta \right]_t$$

$$+ fH_1 H_x\eta_y = \frac{f^2}{g'H_2}H_x\psi_y. \tag{7}$$

The velocity components in each layer are related to ψ and η through

$$Hu_1 = -\left[\psi_y - \frac{g'H_2}{f^2}(\eta_{xt} + f\eta_y) \right] \tag{8a}$$

$$Hv_1 = -\left[-\psi_x - \frac{g'H_2}{f^2}(\eta_{yt} - f\eta_x) \right] \tag{8b}$$

$$Hu_2 = -\left[\psi_y + \frac{g'H_1}{f^2}(\eta_{xt} + f\eta_y) \right] \tag{8c}$$

$$Hv_2 = -\left[-\psi_x + \frac{g'H_1}{f^2}(\eta_{yt} - f\eta_x) \right]. \tag{8d}$$

3. A thin upper layer

When considering wave propagation along the channel axis, (6) and (7) are reduced to coupled ordinary differential equations by the carrier wave transformation

$$\psi(x, y, t) = \text{Re}[F(x) \cdot \exp(iky - i\omega t)] \tag{9a}$$

$$\eta(x, y, t) = \text{Re}[G(x) \cdot \exp(iky - i\omega t)] \tag{9b}$$

where $\omega > 0$.

Allen (1975), following Buchwald and Adams (1968), considered an exponential depth of the form $H_2 \sim \exp(x/L)$ which ensures that the coupled ordinary differential equations for $F(x)$ and $G(x)$ have constant coefficients. On the continental shelf, the situation considered by Allen, $L \approx 100$ km, the width of the shelf, which is also the offshore length scale of barotropic shelf waves. Baroclinic Kelvin waves (the other mode) are trapped within one internal Rossby radius of the coast [Ri = $(g'D_1 D_2/f^2 D)^{1/2}$], with Ri ≈ 15 km. Under these circumstances, Allen introduced the small parameter $\epsilon = \text{Ri}/L \ll 1$ and sought solutions for $F(x)$ and $G(x)$ such that for scales of motion larger than $O(L)$,

$$F(x) = \sum_{n=0}^{\infty} \epsilon^n F_n(x) = O(1)$$

$$G(x) = O(\epsilon^2),$$

corresponding to an $O(1)$ shelf wave coupled to an $O(\epsilon^2)$ baroclinic motion. Similarly, an $O(1)$ baroclinic Kelvin wave would then be coupled to an $O(\epsilon)$ barotropic motion. For lengths shorter than $O(L)$, the shelf wave and the Kelvin wave are fully coupled. At very short wavelengths, Allen found that the motion is bottom trapped.

For the narrow channels in which we are interested, of width $L = O(\text{Ri})$, an expansion in a power series of $\epsilon = \text{Ri}/L$ is clearly not indicated. Similarly, the scaling $L/\lambda \ll 1$ used by Allen and Romea (1980) to describe waves of horizontal long-channel scales much larger than the channel width is not applicable here. We shall choose a scaling based on different circumstances, as follows. We first introduce the nondimensional variables

$$\sigma = \omega/f, \quad k' = kL, \quad x' = x/L, \quad t' = tf$$

$$u_i' = u_i/U, \quad v_i' = v_i/U, \quad h = H/D, \quad h_2 = H_2/D_2$$

$$G' = G/N, \quad F' = F/Q. \tag{10}$$

The scales Q and N will be specified later, but are chosen so that $G = O(F) = O(1)$; U is the horizontal velocity scale. Substituting for ψ and η in terms of (9) in (6) and (7), we find, after dropping the primes, the pair of coupled ordinary differential equations in nondimensional coordinates

$$F_{xx} - \frac{h_x}{h} F_x - \left[k^2 + \frac{kh_x}{\sigma h}\right]F = -\frac{g'H_1}{f}\frac{N}{Q}\frac{h_x}{h}\frac{k}{\sigma}G$$

$$\text{(11a)}$$

$$G_{xx} + \frac{H_1}{D_2}\frac{h_x}{h_2 h}G_x - \left[k^2 + \frac{L^2 h}{h_2 \text{Ri}^2} - \frac{H_1}{D_2}\frac{k}{\sigma}\frac{h_x}{hh_2}\right]G$$

$$= \frac{-f}{g'D_2}\frac{Q}{N}\frac{h_x}{hh_2}\frac{k}{\sigma}F. \quad \text{(11b)}$$

For the chosen scaling, all four terms on the left-hand side of (11a) are of the same order. The first and the third arise from local changes in the vertically integrated vorticity; the other two result from vortex stretching related to the bottom slope. In order to be of comparable significance, the inhomogeneous coupling term must be of similar order; comparing it with the last term on the other side of (11a), this will be so whenever $g'H_1/f = Q/N$. A similar argument applied to the second equation requires that $g'D_2/f = Q/N$ for full coupling. Thus, both coupling terms are of similar significance only when $H_1 = O(D_2)$, i.e. when both layers are of comparable thickness.

In many coastal environments, the density stratification naturally separates the water column into a relatively thin (20–50 m) upper layer overlying a significantly deeper denser layer. In this case, the one of interest here, only one of the equations (11) has an O(1) coupling term. Given $H_1/D_2 \ll 1$, it now remains to choose a consistent scaling for Q and N, whose ratio will determine the relative importance of the inhomogeneous terms in (11). The two possible choices for the ratio Q/N are

$$Q/N = g'D_2/f \quad \text{(12a)}$$

$$Q/N = g'D_1/f. \quad \text{(12b)}$$

The first choice yields an O(1) coupling term in (11b) and a small, $O(H_1/D_2)$ inhomogeneous term in (11a). The system of equations then describes a free "barotropic" mode (11a), which forces a baroclinic response through the effect of vortex stretching in the topographic coupling term in (11b). The other choice of Q/N, as we shall see, is inconsistent with the scaling chosen. The "thin upper layer" approximation was also invoked by Allen and Romea (1980) in a model obeying $L/\lambda \ll 1$ of waves over an exponential bathymetry.

A reasonable scaling for Q, representing the integrated mass-transport stream function, is $Q = DUL$. Two possible choices of N follow from (12). In the first case, $N = Qf/g'D_2$, and the equations (11) become

$$hF_{xx} - h_x F_x - \left(k^2 + \frac{k}{\sigma}h_x\right)F = O\left(\frac{H_1}{D_2}\right) \quad \text{(13a)}$$

$$G_{xx} - \left(k^2 + \frac{L^2}{\text{Ri}^2}\right)G = -\frac{k}{\sigma h h_2}h_x F + O\left(\frac{H_1}{D_2}\right). \quad \text{(13b)}$$

Correspondingly, the velocity components are expressed as

$$hu_1 = [kF - h_2(-\sigma G_x + kG)]\sin(ky - \sigma t) \quad \text{(14a)}$$

$$hv_1 = [F_x + h_2(G_x - k\sigma G)]\cos(ky - \sigma t) \quad \text{(14b)}$$

$$hu_2 = \left[kF - \frac{H_1}{D_2}(-\sigma G_x + kG)\right]\sin(ky - \sigma t) \quad \text{(14c)}$$

$$hv_2 = \left[F_x + \frac{H_1}{D_2}(G_x - k\sigma G)\right]\cos(ky - \sigma t). \quad \text{(14d)}$$

Since $h_2 \sim O(1)$, whereas $H_1/D_2 \ll 1$, the upper layer motions may depart significantly from the barotropic solution (with the possibility of surface intensification if the signs are right), whereas the lower layer flows do not.

For the other choice of Q/N, given by (12b), a similar analysis leads to velocity components of the form

$$hu_1 = \left[kF + \frac{D_2}{H_1}(-\sigma G_x + kG)\right]\sin(ky - \sigma t),$$

i.e., $u_1 = O(D_2/H_1) \gg 1$, in contradiction to the scaling which started with non-dimensional velocity components as O(1) variables. The scaling to be adopted for $H_1/D_2 \ll 1$ must then be that leading to (17)–(19). The uncoupled barotropic wave described by (13a) depends on the form of the bottom profile $h(x)$; the coupled interfacial motion which it drives through the coupling term in (13b) will be described by the latter's particular solution:

$$G(x) = \frac{1}{2\gamma}\{e^{-\gamma x}[R - I(x)] + e^{\gamma x}[S - J(x)]\} \quad \text{(15)}$$

where

$$\gamma^2 = (k^2 + L^2/\text{Ri}^2) \quad \text{(16a)}$$

$$I(x) = -\int_0^x \frac{k}{\sigma}\frac{h_\xi}{h}\frac{F(\xi)}{h_2}e^{\gamma\xi}d\xi \quad \text{(16b)}$$

$$J(x) = -\int_0^x \frac{k}{\sigma}\frac{h_\xi}{h}\frac{F(\xi)}{h_2}e^{-\gamma\xi}d\xi \quad \text{(16c)}$$

and where the constants R and S are determined from the conditions that the normal velocity components $u_1(x)$ and $u_2(x)$ vanish on the boundaries at $x = \pm 1$:

$$R = \frac{-1}{2\sinh(2\gamma)}\left\{\begin{matrix}[1 - k/\gamma\sigma]\\[1 + k/\gamma\sigma]\end{matrix}[J(1) - J(-1)]\right.$$

$$\left. + [I(1)e^{-2\gamma} - I(-1)e^{2\gamma}]\right\} \quad \text{(17a)}$$

$$S = \frac{-1}{2\sinh(2\gamma)}\left\{\begin{matrix}[1 + k/\gamma\sigma]\\[1 - k/\gamma\sigma]\end{matrix}[I(1) - I(-1)]\right.$$

$$\left. + [J(1)e^{2\gamma} - J(-1)e^{-2\gamma}]\right\}. \quad \text{(17b)}$$

The problem thus consists in solving for $F(x)$ given a depth profile $h(x)$. The other part of the solution, $G(x)$ then follows from the preceding relations. We do not consider internal Kelvin wave modes. With the parameter range we are using, their speed is of $O(1)$, always larger than the speed of the topographic modes. Therefore no modal splitting can occur, since the dispersion curves never intersect.

4. Linear bottom profile

We obtain solutions of (13a) for two specific depth profiles: an asymetric V-shaped channel with linear slopes described by

$$h(x) = 1 - s\|x\| \qquad (18)$$

where $s = s_1$ for $x \geq 0$, s_2 for $x \leq 0$, and a symmetric parabolic profile given by

$$h(x) = 1 - sx^2. \qquad (19)$$

In all cases $0 < s < 1$ to ensure that $0 < h(x) < 1$ within the channel.

The walls of the channel are located at $x = \pm 1$; the normal velocity component u must vanish there in both layers. Pressure and normal transport must remain continuous in each layer at the discontinuity in bottom slope found on the channel axis ($x = 0$) for profile (18). We shall extend the analysis to strong bottom slopes, with $s = O(1)$. This will allow us to examine the range of validity of the commonly used "small-slope" approximation, wherein $h(x)$ is assumed constant except when differentiated.

a. Small slope approximation

For $s \ll 1$, substitution of (18) in (13a) yields, to $O(s)$,

$$F_{xx}^+ + s_1 F_x^+ + (s_1 k/\sigma - k^2)F^+ = 0, \quad x \geq 0 \qquad (20a)$$

$$F_{xx}^- - s_2 F_x^- + (-s_2 k/\sigma - k^2)F^- = 0, \quad x \leq 0. \qquad (20b)$$

Solutions satisfying the boundary and matching conditions are

$$F^+(x) = -E \sinh(\delta) \sin[\theta(x - 1)]e^{-s_1 x/2} \qquad (21a)$$

$$F^-(x) = E \sin(\theta) \sinh[\delta(x + 1)]e^{+s_2 x/2} \qquad (21b)$$

where E is an amplitude constant and θ and δ, defined by

$$\theta^2 = s_1 k/\sigma - k^2 - s_1^2/4 \qquad (22a)$$

$$\delta^2 = s_2 k/\sigma + k^2 + s_2^2/4, \qquad (22b)$$

are related through the dispersion relation

$$(s_1 + s_2)/2 + \theta \cot(\theta) + \delta \coth(\delta) = 0. \qquad (23)$$

For $k > 0$, $\delta^2 > 0$, $\theta^2 > 0$ is also required to satisfy boundary conditions. In that case, waves travel in the positive y-direction and exhibit oscillatory behavior on

the right-hand side of the channel ($x > 0$) and are exponentially decaying on the other side. This behavior is reversed for waves traveling in the other direction. Dispersion curves for the first three cross-channel modes are shown in Fig. 2a for $s_1 = s_2 = 0.26$ (for which the small slope approximation should be valid) and in Fig. 3a for $s_1 = s_2 = 0.75$ (for which it should not).

b. Large bottom slope

When $s = O(1)$, $h(x)$ can no longer be approximated by some constant value. The governing equation (13) can be transformed into a pair of confluent hypergeometric equations by defining the new variables

$$q^+(z) = (F(x)e^{z_1/2})/h^2, \quad z_1 = 2k(1 - s_1 x)/s_1, \quad x \geq 0 \qquad (24a)$$

$$q^-(z) = (F(x)e^{z_2/2})/h^2,$$

$$z_2 = -2k(1 - s_2 x)/s_2, \quad x \leq 0. \qquad (24b)$$

We shall consider only the case $s_1 = s_2 = s$, corresponding to $z_1 = -z_2 = z$, for which

$$zq_{zz}^+ + (3 - z)q_z^+ - (3/2 - 1/2\sigma)q^+ = 0, \quad x \geq 0, \qquad (25a)$$

$$zq_{zz}^- + (3 + z)q_z^- - (3/2 - 1/2\sigma)q^- = 0, \quad x \leq 0. \qquad (25b)$$

The general solution of (25a) is expressed in terms of the linearly independent Kummer functions M and U (Abramowitz and Stegun, 1974, p504):

$$q(z) = A \cdot M[a; b; z] + B \cdot U[a; b; z] \qquad (26)$$

where

$$a = (3/2 - 1/2\sigma), \quad b = 3. \qquad (27)$$

Since b is an integer, U has a logarithmic singularity at $z = 0$. However $z > 0$ everywhere within the channel (z represents the depth times a positive constant), so that $U[a; b; z]$ remains analytic everywhere within the domain of interest. The function $M[a; b; z]$ has oscillatory or exponential character depending on the sign of a. $M[a; b; z]$ has zero crossings (required to satisfy the wall boundary conditions) only if $a < 0$. There is thus an upper bound to the frequency of the waves considered, given by

$$\sigma < 1/3 \quad (a \text{ must be negative}). \qquad (28)$$

This agrees with Reid's (1958) short-wave limit for second class barotropic edge waves in a wedge and with Ou's (1980) barotropic limit for coastally trapped waves in a stratified wedge.

For $x \leq 0$, the solution of (25b) is

$$q^-(z) = C \cdot M[a; b; -z] + D \cdot U[a; b; -z]$$
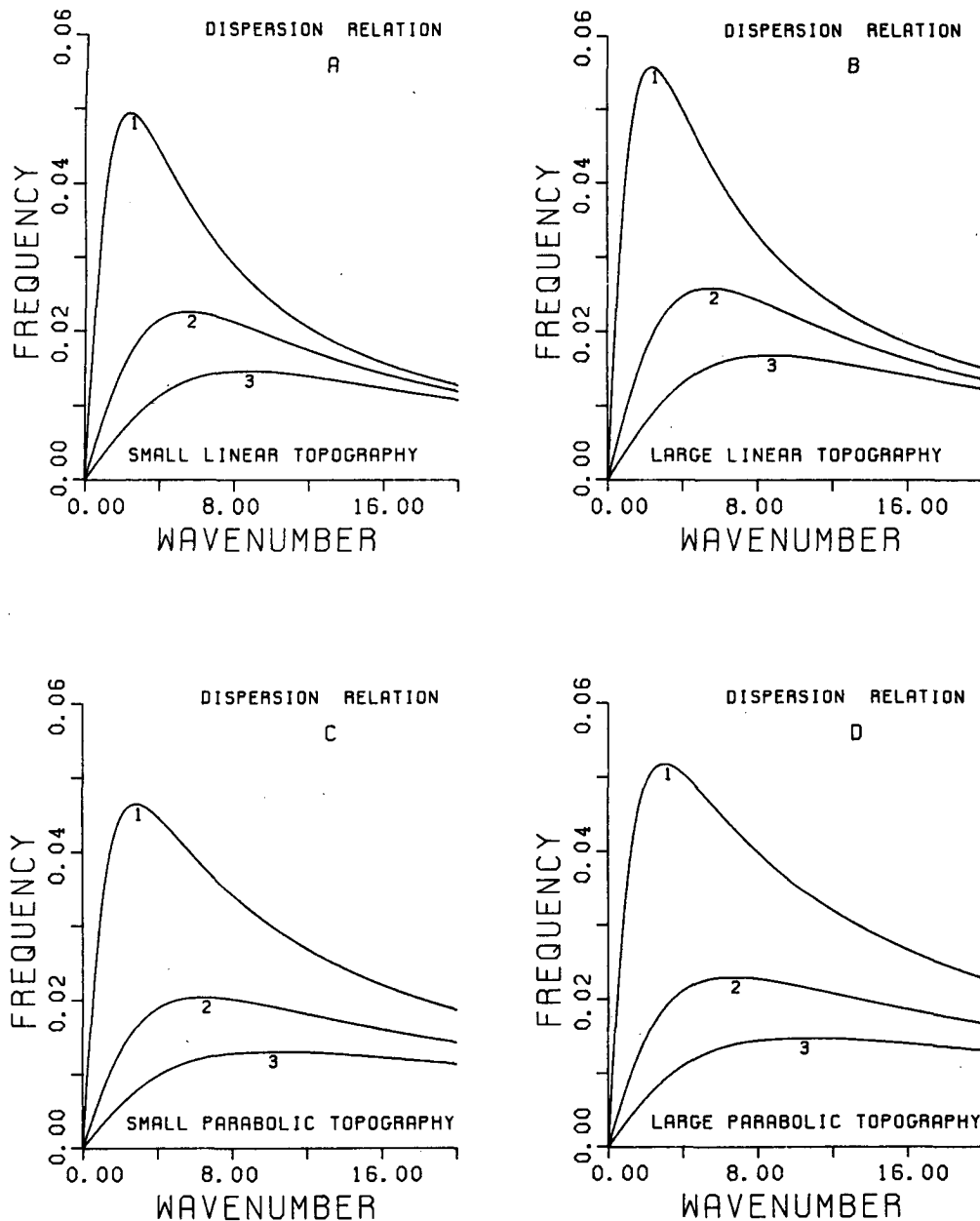
which may be rewritten, using Kummer's transformation, as

FIG. 2. Dispersion diagrams for the four bottom profiles studied. The nondimensional slope is $s = 0.26$. Small linear (parabolic) topography refers to results obtained following the approximate method of sections 4a and 5a; large linear (parabolic) topography results are obtained, for the same bottom slopes, by the more precise method of sections 4b and 5b.

$$q^-(z) = e^{-z/2}\{C \cdot M[3 - a; 3; z]$$

$$+ D \cdot U[3 - a; 3; z]\}. \quad (29)$$

For very low frequencies, a is large and negative; $(3 - a)$ is large and positive. When both z and $(3 - a)$ are large and positive, there is no known asymptotic form for M and U (Abramowitz and Stegun, 1964, p512) and the series representation converges very slowly. We have taken advantage of the fact that the solutions $F(x)$ are always analytic inside the channel boundaries to expand in Taylor series about the regular point $x = 0$, rather than in a Frobenius series (the Kummer functions M and U) around the singular point $z = 0$. Dispersion curves for the first three modes are shown in Figs. 2b and 3b for $s = 0.26$ and 0.75, respectively.
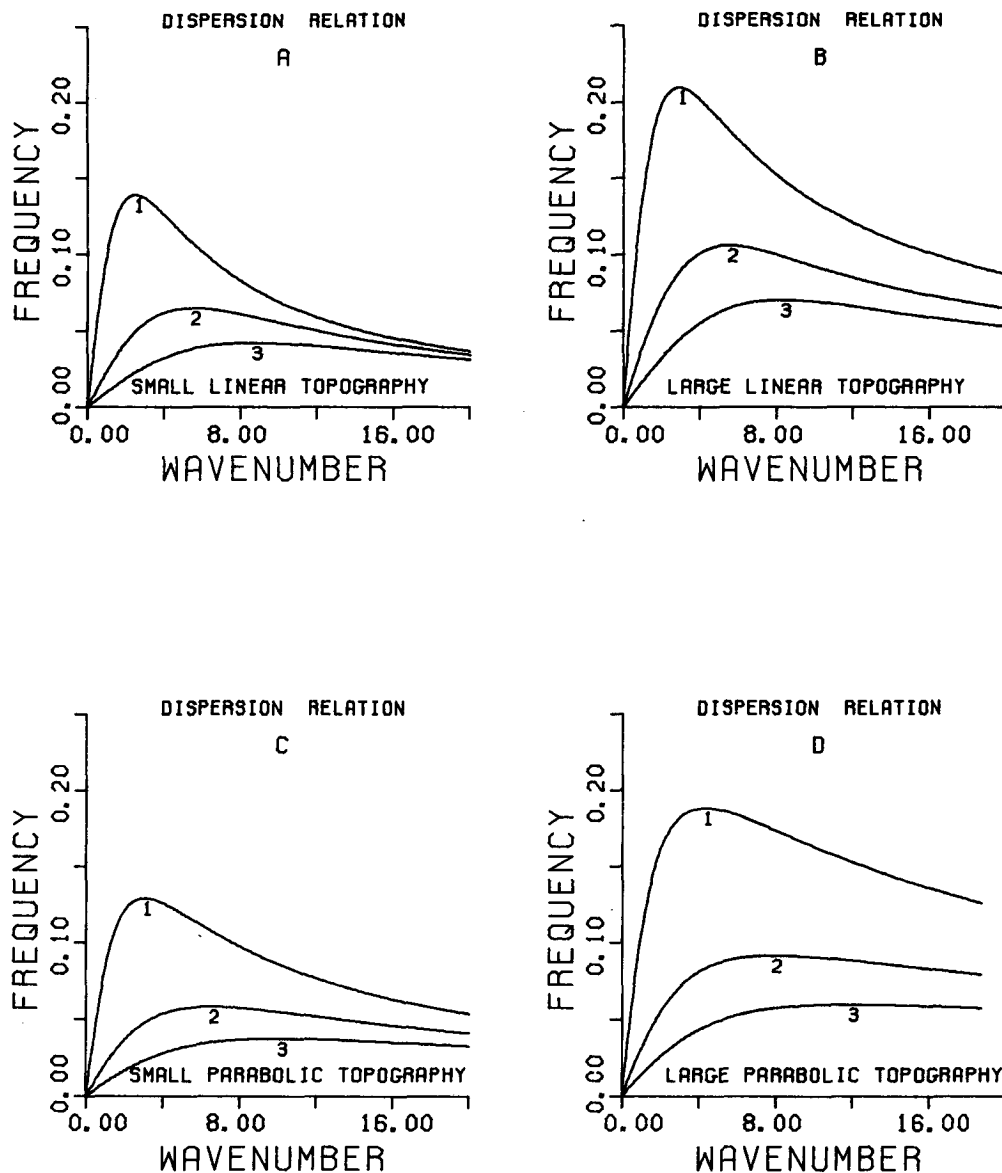
DISPERSION RELATION
A

FREQUENCY

SMALL LINEAR TOPOGRAPHY

WAVENUMBER

DISPERSION RELATION
B

FREQUENCY

LARGE LINEAR TOPOGRAPHY

WAVENUMBER

DISPERSION RELATION
C

FREQUENCY

SMALL PARABOLIC TOPOGRAPHY

WAVENUMBER

DISPERSION RELATION
D

FREQUENCY

LARGE PARABOLIC TOPOGRAPHY

WAVENUMBER

FIG. 3. As in Fig. 2 but for $s = 0.75$.

5. Parabolic bottom profile

The analysis of the propagation of coupled bathymetric-stratification waves in a channel with a parabolic bottom profile described by (19) follows that described for the linear profile: results are obtained first under the small-slope approximation, followed by the exact solutions. In this case, analytic expressions for $F(x)$ may be found in terms of parabolic cylinder functions under the small-slope approximation and of generalized spheroidal wave functions (Wilson, 1928) otherwise. That representation is given in Gratton (1983), where it is also shown that for the range of parameter

values of interest eigenfunctions and frequencies are more conveniently computed through Taylor function expansions.

a. Small-slope approximation

Substitution of (19) into (17a) yields

$$F_{xx} + 2sxF_x + (2ksx/\sigma - k^2)F = 0. \qquad (30)$$

The solution which satisfies the boundary conditions is (cf. Appendix)

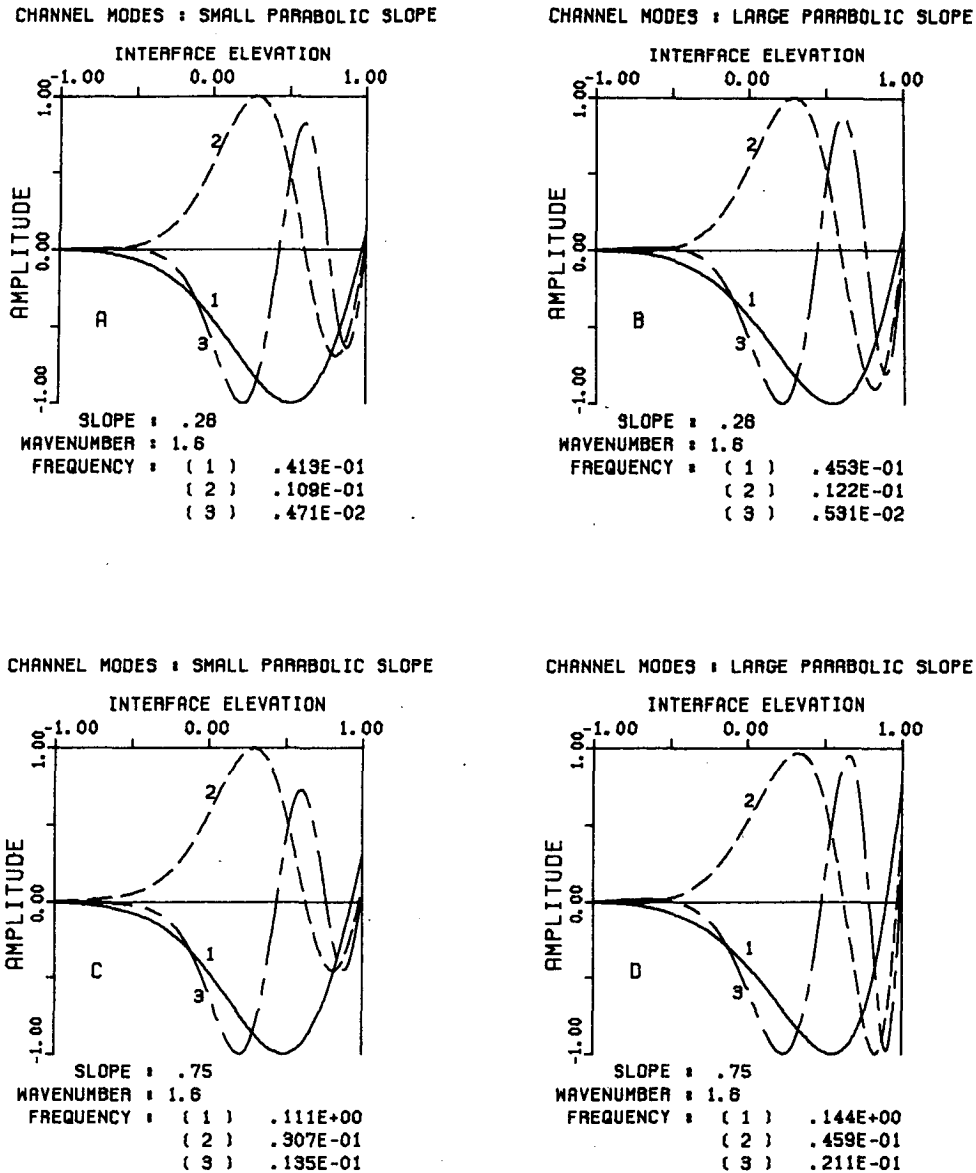$$F(x) = A_0 \cdot SPC(s, x) + B_0 \cdot SPD(s, x) \qquad (31)$$

FIG. 4. Cross-channel structure of the interface elevation over a parabolic bottom with the small slope approximation. (a) $s = 0.26$ and (c) $s = 0.75$; without the small slope approximation (b) $s = 0.26$ and (d) $s = 0.75$. $L/\mathrm{Ri} = 1.0$.

where SPC and SPD (SP = "Small Parabolic" slope) are the two orthogonal infinite series solutions. The coefficients A_0 and B_0 are given by $A_0 = \mathrm{SPD}(s, 1)$; $B_0 = \mathrm{SPC}(s, 1)$, and the dispersion relation is expressed as

$$B_0 \cdot \mathrm{SPD}(s, -1) - A_0 \cdot \mathrm{SPC}(s, -1) = 0. \quad (32)$$

Dispersion curves are shown in Figs. 2c and 3c. They resemble those obtained in the linear case; for a given wavenumber, the eigenfrequencies lie between those obtained for the small and large linear slopes.

b. Large bottom slope

For strong parabolic slopes, the solution of (13a) becomes, using the method discussed in the Appendix

$$F(x) = h^2[A_0 \cdot \mathrm{LPC}(s, x) - B_0 \cdot \mathrm{LPD}(s, x)] \quad (33)$$

where LPC and LPD (LP = "Large Parabolic" slope) are the two orthogonal series solutions and the coefficients A_0 and B_0 are given by $A_0 = \mathrm{LPD}(s, 1)$; $B_0 = \mathrm{LPC}(s, 1)$. The dispersion relation is written as

$$B_0 \cdot \mathrm{LPD}(s, -1) - A_0 \cdot \mathrm{LPC}(s, -1) = 0 \quad (34)$$

and dispersion curves are shown in Figs. 2d and 3d. Their shapes are similar to those found earlier. For each wavenumber the frequency is higher than that obtained using the small-slope approximation, the differences varying from 5% for $s = 0.1$ to 30% for $s = 0.8$. Moreover, at each wavenumber, the frequencies are lower than those given by the large linear slope model. This result is consistent with the fact that the cutoff frequency is lower for a large parabolic profile ($\frac{1}{4}$) than for large linear profiles ($\frac{1}{3}$). The cutoff frequency is obtained by manipulating (13a) into a generalized spheroidal wave equation (Wilson, 1928). The upper bound for the frequency is then derived from the requirement that the solution must be oscillatory to satisfy the wall boundary conditions.

6. Discussion

The solutions obtained in the previous section represent topographic waves propagating in an axisymmetric channel with strong linear and parabolic bottom slopes. Because of the uncoupling hypothesis, based on $H_1/D_2 \ll 1$, the propagation is unaffected by the stratification. The interface couples to the basic barotropic mode through the inhomogeneous term in (13b), with solutions $G(x)$ given by (15)–(17). The total field of motion then consists of a linear superposition of the two modes, $G(x)$ and $F(x)$, with horizontal velocity components given in (14).

The structure of the eigenfunctions is illustrated in Fig. 4, for the parabolic bottom profile. Flow patterns in each layer are shown in Fig. 5. The flows are surface-intensified because of the nature of the baroclinic component which equilibrates horizontal transports between a thin upper layer and a thick deeper layer with appropriately stronger flows in the former. The behavior of the cross-channel dependence is oscillatory on the side of the channel which is to the right of the direction of wave propagation, and decaying on the other side, where the slope changes side. The rotary current pattern does not change direction with depth.

The influence of the bathymetric shape and of the strength of the bottom slopes on the dispersion curves is seen in Fig. 2 (for which $s = 0.26$) and Fig. 3 ($s = 0.75$). In all cases, the waves are nondispersive at very low frequencies; there is also in every case a wavenumber at which the group velocity vanishes. Figure 6 shows how the frequency varies with the strength of the slope for a choice of three wavenumbers (1.5, 3.0, 6.0) for each model considered. The frequency ratio plotted is equal to the frequency normalized by its value at $s = 0.1$ for each model. The curves $k = 3.0$ and 6.0 are displaced upwards by one and two units respectively to distinguish them from the $k = 1.5$ curve and from each other. A few nonnormalized frequency values are also given in Table 1. We note that the frequency grows a bit faster with s over a linear than over a parabolic
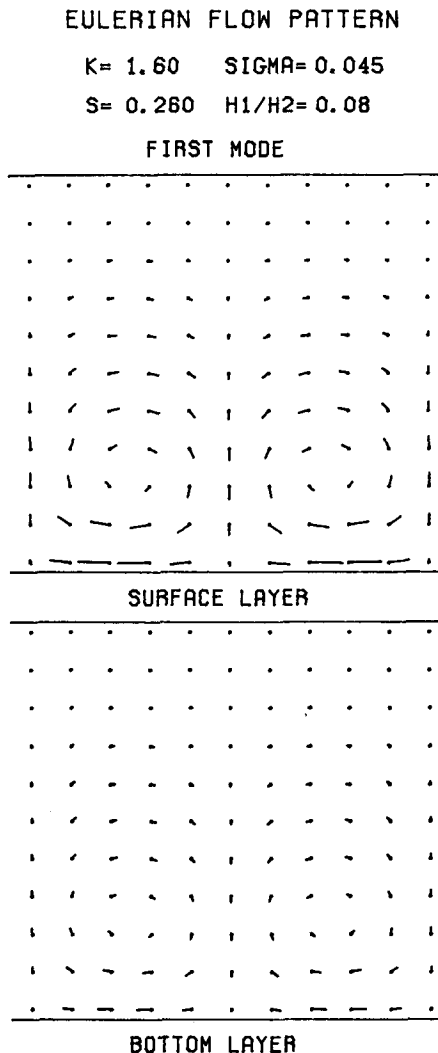

FIG. 5. Eulerian flow in both layers corresponding to the first mode of Fig. 4a.

profile. We also notice that the small-slope approximation systematically underestimates the frequency. The error grows with s and may reach up to 80% when $s = 0.8$, depending on the wavenumber.

Table 2 gives values of the frequency and wavenumber at which the group velocity of the first mode vanishes. Both grow with s. Stronger slopes (larger s) thus generally stiffen the system and displace the dispersion curve towards higher wavenumber and frequencies. Thus, for instance, over a parabolic profile with $s = 0.7$ in a channel of width 20 km, the shortest wave period is about 4 days, with a wavelength of about 20 km.

The shape of the eigenfunctions is also sensitive to the value of the bottom slope. As seen in Fig. 4, for both methods of calculation, it is clear that larger bottom slopes increase the interfacial displacement ob-
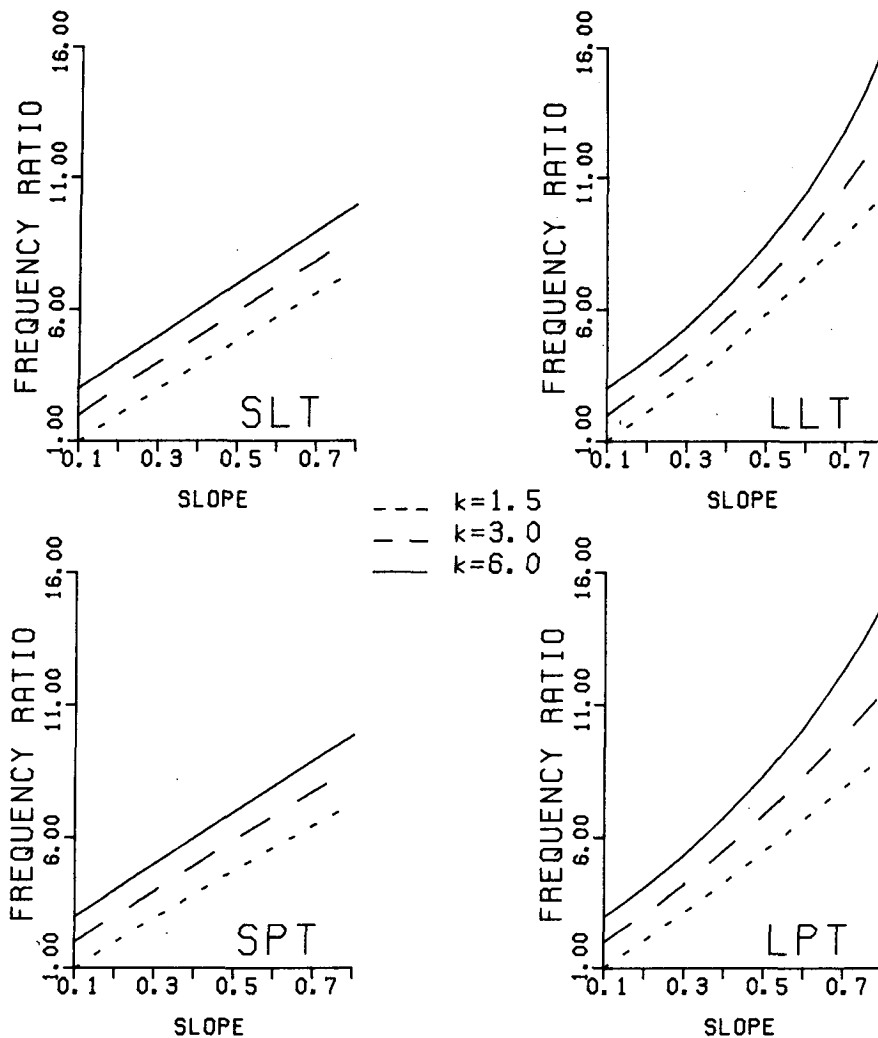
FIG. 6. Plots of frequency versus slope for small linear (SLT), large linear (LLT), small parabolic (SPT), and large parabolic (LPT) topographies, for three different wave numbers (k = 1.5, 3.0, 6.0).

served at the right-hand boundary compared to its midchannel maxima. The effect of the small-slope approximation is also strikingly evident (compare Figs. 4a with 4b and 4c with 4d) in its underestimation of the strength of interfacial oscillations on the right-hand side of the channel. Similar results prevail over the linear bottom profiles.

Our results clearly show the inadequacy of the small-slope approximation as soon as s exceeds about 0.2. Keeping the full cross-channel dependence in h of course complicates matters and, except for a few special profiles, makes it impossible to express $F(x)$ in terms of known analytical functions. Our experience with the linear and parabolic profiles has shown, moreover, that for the range of parameters of interest, it was simpler to work with Taylor series solutions than to try and estimate the higher transcendental functions in-

volved. In channels where the depth does not vanish, no singularities are found within the boundaries, and solutions of (13a) may be obtained by Taylor expansions about the channel axis (x = 0). This method may be trivially extended, for axially unbounded rectilinear channels to depth profiles of the form

$$h(x) = e^{bx}(1 - \sum_{n=0}^{N} a_n x^n). \qquad (35)$$

It should thus be possible to model more closely the bathymetry of long channels and obtain solutions for wave propagation, using the method described in the Appendix, without need for the small-slope approximation.

Our solutions are of course appropriate only for a two-layer fluid, and rely on assuming that the upper

TABLE 1. Frequencies computed with the small linear (SLT), large linear (LLT), small parabolic (SPT), and large parabolic (LPT) topography models, at the same wavenumber ($k = 1.6$). All variables are dimensionless.

	s		
	0.20	0.50	0.80
First mode			
SLT	0.0356	0.0869	0.1352
LLT	0.0389	0.1096	0.1977
SPT	0.0320	0.0768	0.1178
LPT	0.0344	0.0920	0.1538
Second mode			
SLT	0.0096	0.0237	0.0376
LLT	0.0106	0.0317	0.0652
SPT	0.0084	0.0207	0.0327
LPT	0.0091	0.0263	0.0508
Third mode			
SLT	0.0041	0.0102	0.0163
LLT	0.0046	0.0139	0.0298
SPT	0.0036	0.0090	0.0143
LPT	0.0040	0.0116	0.0236

layer is thin compared to the subjacent one. The partially uncoupled problem solved is the first-order solution in a regular perturbation series in H_1/D_2. The error is of course worst near the boundaries, where the depth profile ratio is largest. A precise estimate of the error associated with the inequality $H_1/D_2 \ll 1$ not being satisfied in relatively narrow nearshore strips would require a comparison with fully coupled solutions of (13a)–(13b), as in the numerical model of Wang (1975). Comparison of our solutions with those obtained numerically by Lie and El-Sabh (1983) for the St. Lawrence estuary has shown the usefulness of the thin-upper-layer approximation used here.

7. Applications

a. The Strait of Georgia

This study was originally motivated by the need to explain the nature of low-frequency variability observed in the Strait of Georgia (Chang et al., 1976; Yao et al., 1982). Earlier analysis (Helbig, 1978; Helbig and Mysak, 1976), based on a very small slope approximation and the absence of coupling between stratification and bathymetry yielded bottom-trapped motions with long-channel scales much too large to fit into the Strait of Georgia for the range of periods observed (5–50 days). Further examination of the available current data (Schott and Mysak, 1980) has failed to reveal any evidence of phase propagation. Although current thought (LeBlond 1983) seems to lean towards an interpretation of the low-frequency motions in terms of quasi-geostrophic turbulence, it is instructive to examine the nature of the low-frequency waves predicted by our model.

The general bathymetry of the central Strait of Georgia is shown in Fig. 7. A bathymetric section along line H is illustrated in Fig. 8, together with the fits used in our model (solid line) and in that of Helbig and Mysak (1976) (dashed line). The origin of our coordinate system is set at the point of maximum depth ($D = 375$ m). Side boundaries are situated near Sturgeon bank ($x = L_1 = 16$ km) and Valdes Island ($x = -L_1/2$). The actual geometrical slopes are $s_1^* = 1.35 \times 10^{-2}$ and $s_2^* = 2.3 \times 10^{-2}$ on the $x > 0$ and $x < 0$ sides of the channel respectively. In the nondimensional form (18), with respect to the appropriate width on each side of the channel (so that $\|x\| = 1$ on each side), the scaled slopes entering the bilinear profile (18) are respectively $s_1 = 0.6$ and $s_2 = 0.5$. The Coriolis parameter, f, is 1.2×10^{-4} and the internal Rossby radius is 8.1 km.

Dispersion curves for the right-bounded and left-bounded waves are shown in Fig. 9; the asymmetry of the channel is reflected in the difference between the dispersion curves for left-bounded and right-bounded waves. Dispersion curves for symmetric channels with slope $s = 0.5$, 0.6 are also shown for comparison; they are of course the same for both directions of propagation. A glance at Table 3 shows that the shortest possible periods (at the peak of the $\sigma(k)$ curve for the first mode) are about 5 days for right-bounded waves and 6 days for left-bounded waves, corresponding to wavelength of about 36 km and 17 km, respectively.

TABLE 2. Frequency and wavenumber at which the group velocity of the first mode vanishes.

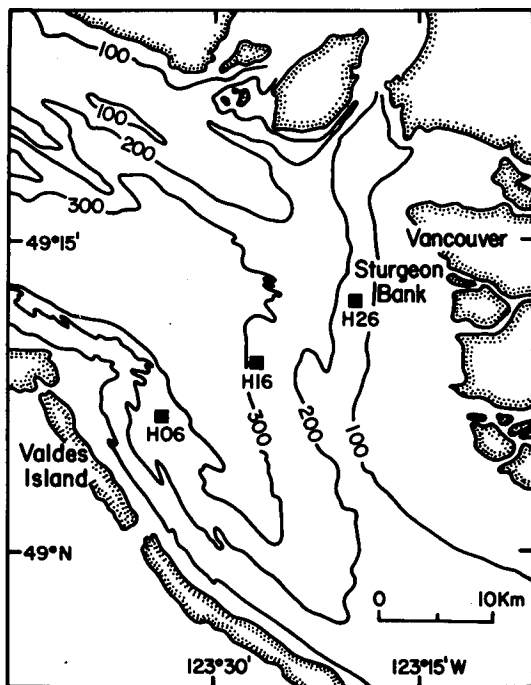|	SLT		LLT		SPT		LPT	
s	σ	k	σ	k	σ	k	σ	k
0.1	0.0191	2.3	0.0199	2.4	0.0180	2.8	0.0188	2.8
0.2	0.0381	2.4	0.0417	2.4	0.0358	2.8	0.0389	2.9
0.3	0.0569	2.4	0.0654	2.4	0.0534	2.9	0.0605	3.1
0.4	0.0754	2.4	0.0914	2.5	0.0706	2.9	0.0840	3.2
0.5	0.0938	2.4	0.1203	2.6	0.0876	3.0	0.1096	3.4
0.6	0.1119	2.5	0.1526	2.7	0.1033	3.0	0.1381	3.7
0.7	0.1299	2.5	0.1893	2.8	0.1208	3.0	0.1699	3.9
0.8	0.1476	2.5	0.2317	3.0	0.1370	3.1	0.2070	4.7

FIG. 7. Bathymetric contours (in meters) of the Central Strait of Georgia. Location of moorings line H is also shown.

A model which includes a significant bathymetric influence on interfacial motion, i.e., a forcing of the baroclinic mode by a traveling barotropic wave, reproduces the surface intensified flow observed at low frequencies in the Strait of Georgia; it also yields horizontal scales of motion which fit readily in the Strait for the observed range of periods and are more in keeping with the short correlation scales ($L_c \approx 5$ km) observed. It is imaginable that superpositions of a few modes traveling in each direction might, if they were uncorrelated with each other, be consistent with the available observations. A much more ambitious sampling program, now in progress, may yet reveal some phase propagation through a large array located in the central Strait, for which the waves discussed here would provide an improved model.

b. The Saint Lawrence estuary

The bathymetry of the lower St. Lawrence estuary consists of a deep channel (Fig. 10) in which there has also been observed a subinertial current variability (El-Sabh et al. 1982). Lie and El-Sabh (1983) have presented a numerical model of wave propagation in a two-layer channel with bottom profile

$$H_2(x) = H_0 - \sin[(10\pi/4)(1 + x)] \exp(-2x),$$

$$0 \leqslant x \leqslant 0.5 \quad (36a)$$

$$H_2(x) = H_0 - (H_c - H_0)[1 - \sin(x)],$$

$$0.5 \leqslant x \leqslant 1.0 \quad (36b)$$

where H_c is the thickness of the bottom layer at the southern shore (Matane). We have chosen to model the bathymetry with the parabolic profile shown in Fig. 10, with $s = 0.6$; the profile given by (36) is also shown. For the cross section considered the following parameter values hold:

$$D_2 = 300 \text{ m}, \quad H_1 = 45 \text{ m}, \quad H_1/D_2 = 0.18$$

$$f = 10^{-4} \text{ s}^{-1}, \quad j = 4.38 \times 10^{-3}, \quad L = 23 \text{ km}.$$

The internal Rossby radius is 13 km. Because of the difference in bathymetric profiles, we expect our results to differ slightly from those of Lie and El-Sabh (1983). Table 4 presents frequencies for a nondimensional wavenumber $k = 1.6$ (corresponding to waves of length twice the channel width; our scaling differs from that of Lie and El-Sabh: our $k = 1.6$ corresponds to their $k = \pi$). For the homogeneous model, the two sets of frequencies are within 10% of each other, a difference which might be attributed to the difference in bathymetric profiles. The difference is more pronounced in the two-layer model. This is expected since the inclusion of stratification increases the frequency. To give closer results, the first-order correction to the frequency should be included. The calculations of Lie and El-Sabh (1983) are not subject to the $H_1/D_2 \ll 1$ approximation, and the difference which they find between the eigenfrequencies of the two- and one-layer models is an indication of the cross-coupling between (13a) and (13b), which has been eliminated by our thin-upper layer approximation.

8. Summary and conclusions

Low-frequency topographic waves have been known for some time. Lamb (1932, §192, 212) already dis-
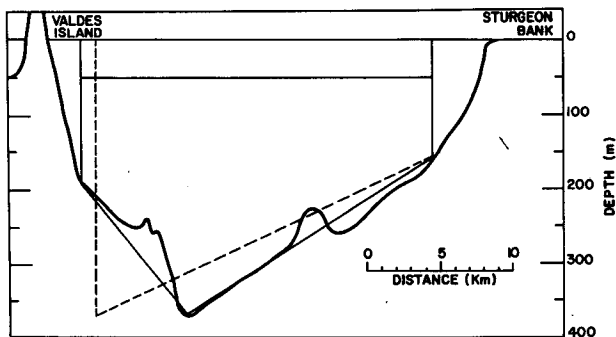

FIG. 8. Bathymetric section along line H (see Fig. 7, for location). The solid line is the fit used in our model and the dashed line is the fit used by Helbig and Mysak (1976). Modified from Helbig (1978).
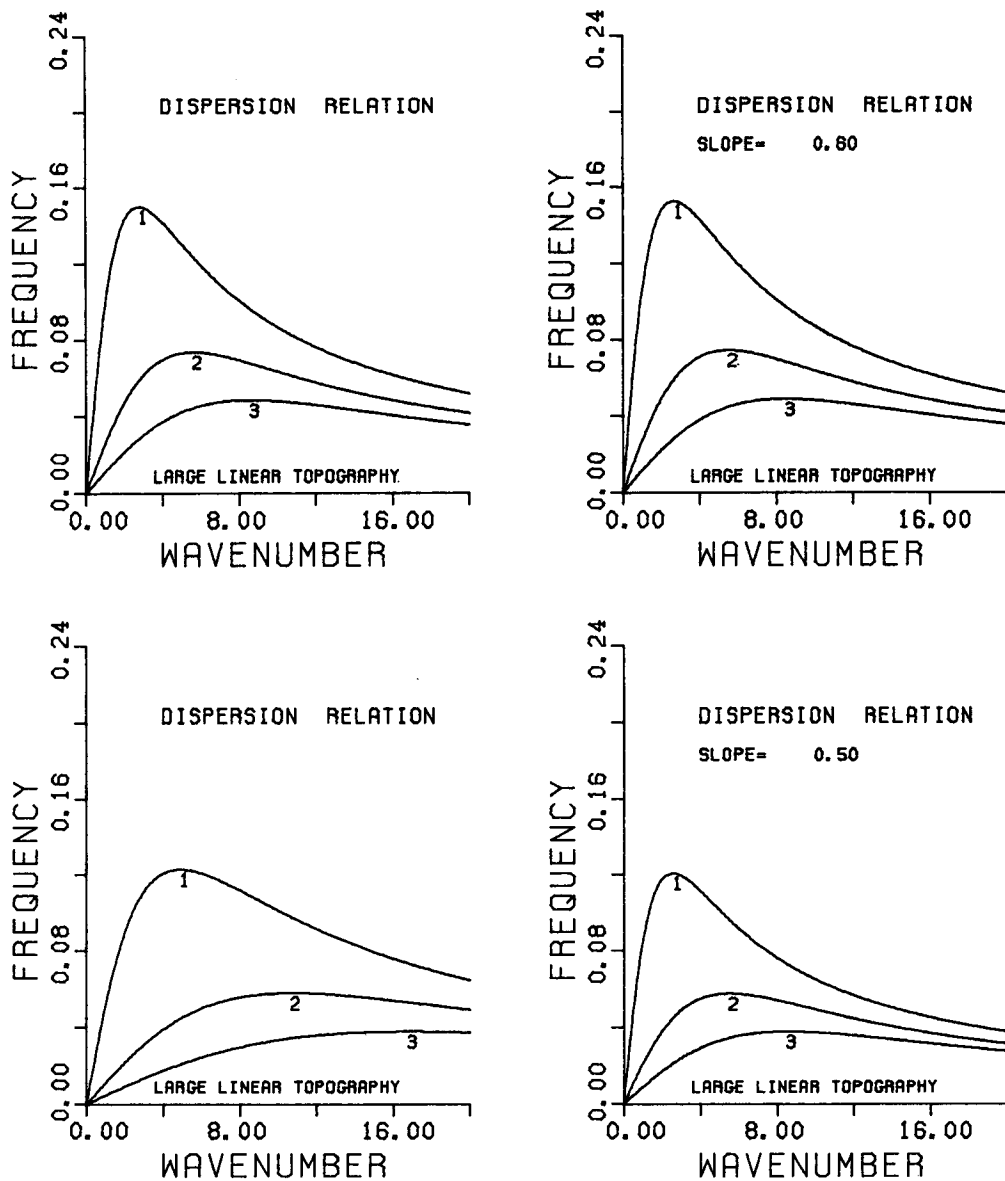
FIG. 9. Dispersion curves for the right-bounded wave (upper left) and the left-bounded wave (lower left) propagating over the bottom profile shown in Fig. 8. The two other curves (upper and lower right) are for waves propagating over the corresponding axisymmetric bottom profiles.

cussed some of their properties. Simple analytical solutions have been found only for special bottom profiles in a homogeneous fluid and especially in the presence of density stratification. For channels and basins, there has been no simple model which represents topographic-mode solutions on a basin-wide scale in a stratified fluid.

We have introduced a different approximation method, applicable to two-layer stratification with a relatively thin upper layer (a not uncommon situation), which allows partial decoupling of topographic and

stratification effects. Two bathymetric profiles (linear and parabolic) have been examined in detail and solutions using a small-slope approximation have been compared to more precise results where this approximation was not used. We found that the small-slope approximation consistently underestimated the frequency of the waves. A Taylor series expansion method was used to obtain streamfunction solutions in the selected profiles; this method was also shown to be applicable to a wide variety of bathymetries (for which the depth never vanishes) obviating the need for the

TABLE 3. Correspondence between the dimensional and nondimensional wavenumbers and frequencies.

k	$2\pi/k$ km	σ	$2\pi/\sigma$ days
2.5	2.5 L	0.02	36.4
3.0	2.1 L	0.07	10.4
3.5	1.8 L	0.17	6.1
4.0	1.6 L	0.17	4.3
4.5	1.4 L	0.22	3.3

TABLE 4. Frequencies computed by Lie and El-Sabh (1983) and with the large parabolic topography model. The wavelength is twice the channel width ($k = 1.6$).

Modes	Lie and El-Sabh (1983)		LPT	
	One-layer	Two-layer	$s = 0.60$	$s = 0.75$
1	0.1248	0.1426	0.1126	0.1438
2	0.0368	0.0456	0.0334	0.0459
3	0.0168	0.0214	0.0149	0.0211

small-slope approximation or the evaluation of higher transcendental functions in untabulated ranges of parameter.

The solutions of the model yield surface intensified sub-inertial motions similar to those observed in the Strait of Georgia (Chang et al., 1976; Yao et al., 1982) and the St. Lawrence estuary (El-Sabh et al., 1982). A comparison to a numerical model of low-frequency motion in the latter estuary (Lie and El-Sabh, 1983) shows good agreement with our approximate semi-analytic solutions.

Such surface-intensified topographic waves also appear to exist in small stratified lakes (Saylor et al., 1980;
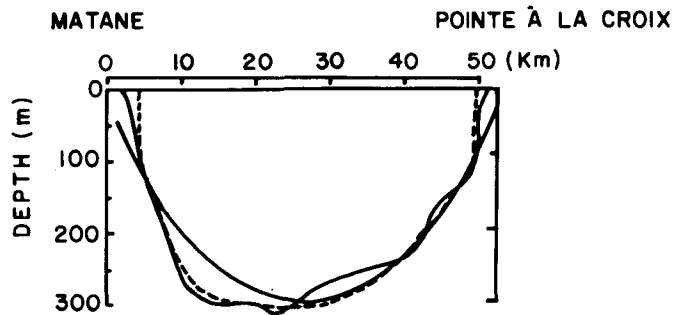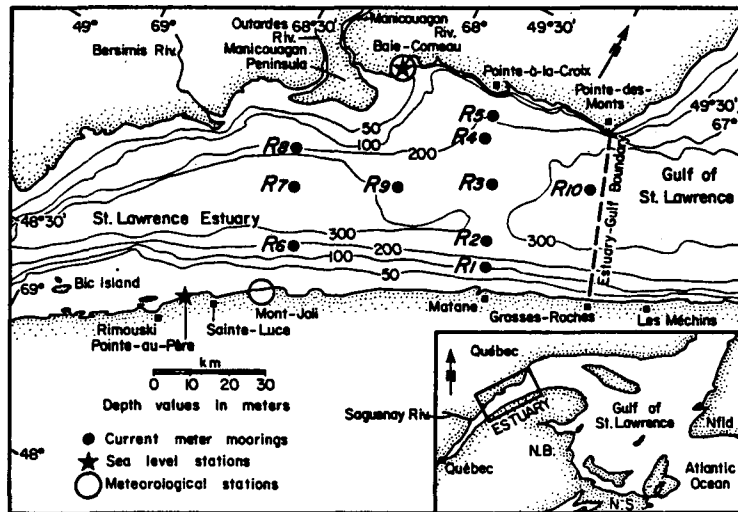

FIG. 10. Location and bathymetry of the Matane-Pointe a la croix section. The dashed line is the fit used by Lie and El-Sabh (1983) and the solid line is the fit used in our model. Modified from Lie and El-Sabh (1983).

Mysak et al., 1983). The analysis was extended to circular lakes by Gratton (1983) and to elliptical lakes by Mysak (1985). This latter model has been successfully used to explain the low-frequency temperature fluctuations observed during the summer of 1979 in Lake of Lugano, Switzerland (Mysak et al., 1984). Topographic waves account for the period, propagation amplitude and structure of the observed thermocline oscillations.

APPENDIX

Taylor Series Solutions

The fundamental equation is

$$hF_{xx} - h_xF_x - [k^2 + (k/\sigma)h_x]F = 0. \qquad (13a)$$

For large, O(1), slopes, it is convenient to first transform (13a) into

$$hq_{xx} + 3h_xq_x + [2h_{xx} - k^2h - (k/\sigma)h_x]q = 0 \qquad (A1)$$

where

$$q(x) = h^2F(x).$$

This transformation greatly simplifies the evaluation of (15).

1. Large linear topography (LLT)

Upon substitution of (18), (A1) becomes

$$(1 - z)q_{zz} - dq_z + (a^2z + b)q = 0, \quad z = sx$$

where $s = s_1$ when $x > 0$ and $s = -s_2$ when $x < 0$. The constants a, b, and d are given by

$$a = k/s, \quad b = a(1/\sigma - a), \quad d = 3.$$

The Taylor series solution is

$$q(z) = A \sum_0^\infty C_nz^n + B \sum_0^\infty D_nz^n.$$

The C_i and the D_i are given by

$$C_0 = 1, \quad D_0 = 0$$
$$C_1 = 0, \quad D_1 = 1$$
$$C_2 = -b/2, \quad D_2 = d/2$$

$$C_n = \{[(n - 1)(n - 2) + d(n - 1)]C_{n-1}$$
$$- bC_{n-2} - a^2C_{n-3}\}/n(n - 1)$$

$$D_n = \{[(n - 1)(n - 2) + d(n - 1)]C_{n-1}$$
$$- bD_{n-2} - a^2D_{n-3}\}/n(n - 1).$$

To standardize the notation, let

$$LLC(s, x) = \sum_0^\infty C_ns^nx^n$$

$$LLD(s, x) = \sum_0^\infty D_ns^nx^n.$$

The two characters LL stand for "Large Linear". Similarly, SP and LP will stand for "Small Parabolic" and "Large Parabolic" respectively. Once the matching conditions are satisfied at the slope discontinuity ($x = 0$), the solution becomes

$$q^+(x) = B_0[A_0LLC(s_1, x) - A_1LLD(s_1, x)], \quad x > 0$$

$$q^-(x) = A_0[B_0LLC(-s_2, x) - B_1LLD(-s_2, x)], \quad x < 0.$$

The A_i and the B_i are given by

$$A_0 = LLD(s_1, 1), \quad A_1 = LLC(s_1, -1)$$

$$B_0 = LLD(-s_2, 1), \quad B_1 = LLC(-s_2, -1)$$

provided that the dispersion relation

$$s_2A_0(B_1 + 2B_0) + s_1B_0(A_1 + 2A_0) = 0$$

is satisfied.

2. Small parabolic topography (SPT)

Substitution of (19) into (13a) yields

$$F_{xx} + dF_x + (ax + b)F = 0$$

where a $2sk/\sigma$, $b = k^2$, and $d = 2s$. The Taylor series solution is

$$F(x) = A \sum_0^\infty C_nx^n + B \sum_0^\infty D_nx^n$$
$$= A_0SPC(s, x) + B_0SPD(s, x).$$

The C_i and the D_i are given by

$$C_0 = 1, \quad D_0 = 0$$
$$C_1 = 0, \quad D_1 = 1$$
$$C_2 = b/2, \quad D_2 = 0$$

$$C_n = \{[b - (n - 2)d]C_{n-2} - aC_{n-3}\}/n(n - 1)$$
$$D_n = \{[b - (n - 2)d]D_{n-2} - aD_{n-3}\}/n(n - 1).$$

3. Large parabolic topography (LPT)

Upon substitution of (19) and using $z = s^{1/2}x$, Eq. (A1) becomes

$$(1 - z^2)q_{zz} - dzq_z + (a^2z^2 + bz + c)q = 0$$

where $a^2 = k^2/s$, $b = 2a/\sigma$, $c = -(4 + a^2)$, and $d = 6$. The Taylor series solution is

$$q(x) = A \sum_0^\infty C_n s^{n/2} x^n + B \sum_0^\infty D_n s^{n/2} x^n$$

$$= A_0 \text{LPC}(s, x) + B_0 \text{LPD}(s, x).$$

The C_i and the D_i are given by

$$C_0 = 1, \qquad D_0 = 0$$

$$C_1 = 0, \qquad D_1 = 1$$

$$C_2 = -c/2, \quad D_2 = 0$$

$$C_3 = -b/6, \quad D_3 = (d - c)/6$$

$$C_n = \{[(n - 2)(n - 3) + (n - 2)b - c]C_{n-2}$$
$$- bC_{n-3} - a^2 C_{n-4}\}/n(n - 1)$$

$$D_n = \{[(n - 2)(n - 3) + (n - 2)b - c]D_{n-2}$$
$$- bD_{n-3} - a^2 D_{n-4}\}/n(n - 1).$$

REFERENCES

Abramowitz, M., and I. A. Stegun, 1964: *Handbook of Mathematical Functions*. Dover, 1046 pp.

Allen, J. S., 1975: Coastal trapped waves in a stratified ocean. *J. Phys. Oceanogr.*, **5**, 300–325.

——, and R. D. Romea, 1980: On coastal trapped waves at low latitudes in a stratified ocean. *J. Fluid Mech.*, **98**, 555–585.

Buchwald, V. T., and J. K. Adams, 1968: The propagation of continental shelf waves. *Proc. Roy. Soc.*, A **305**, 235–250.

Chang, P., S. Pond and S. Tabata, 1976: Subsurface currents in the Strait of Georgia, west of Sturgeon Bank. *J. Fish. Res. Board Can.*, **33**, 2218–2241.

El-Sabh, M. I., H.-J. Lie and V. G. Koutitonsky, 1982: Variability of the near-surface residual circulation in the lower St. Lawrence estuary. *J. Geophys. Res.*, **12**, 9589–9601.

Gratton, Y., 1983: *Low-frequency vorticity waves over strong topography*. Ph.D. Thesis, University of British Columbia, 143 pp.

Helbig, J. A., 1978: *On the inertial stability of coastal flows*. Ph. D. thesis, University of British Columbia, 183 pp.

——, and L. A. Mysak, 1976: Strait of Georgia oscillations: low-frequency currents and topographic planetary waves. *J. Fish. Res. Board Can.*, **33**, 2329–2339.

Hendershott, M. C., 1981: Long waves and ocean tides. *Evolution of Physical Oceanography*, B. A. Warren and C. Wunsch, Eds. MIT Press, 292–341.

Lamb, H., 1932: *Hydrodynamics*, 6th ed. Cambridge University Press, 738 pp.

LeBlond, P. H., 1983: The Strait of Georgia: Functional anatomy of a coastal sea. *Can. J. Fish. Aquat. Sci.*, **40**(7), 1033–1063.

——, and L. A. Mysak, 1978: *Waves in the Ocean*. Elsevier, 602 pp.

Lie, H.-J., and M. I. El-Sabh, 1983: Formation of eddies and transverse currents in a two-layer channel of variable bottom: Applications to the lower St. Lawrence estuary. *J. Phys. Oceanogr.*, **10**, 1063–1075.

Mysak, L. A., 1980: Recent advances in shelf wave dynamics. *Rev. Geophys. and Space Phys.*, **18**, 211–241.

——, 1985: Elliptical topographic waves. *Geophys. Astrophys. Fluid Dyn.*, **31**, 93–135.

——, G. Salvade, K. Hutter and T. Scheiwiller, 1983: Lake of Lugano and topographic waves. *Nature*, **306**(5398), 46–48.

——, ——, ——, and ——, 1984: Topographic waves in a stratified elliptical basin, with application to the Lake of Lugano. *Phil. Trans. Roy. Soc. London A*, in press.

Ou, H. W., 1980: On the propagation of free topographic Rossby Waves near continental margins. Part 1: Analytical model for a wedge. *J. Phys. Oceanogr.*, **10**, 1051–1060.

Pedlosky, J., 1979: *Geophysical Fluid Dynamics*. Springer-Verlag, 624 pp.

Reid, R. O., 1958: Effect of Coriolis force on edge waves, (1) Investigation of the normal modes. *J. Mar. Res.*, **16**, 109–144.

Robinson, A. R., 1964: Continental shelf waves and the response of sea level to weather systems. *J. Geophys. Res.*, **69**, 367–368.

Saylor, J. H., J. C. K. Huang and R. O. Reid, 1980: Vortex modes in southern Lake Michigan. *J. Phys. Oceanogr.*, **10**, 1814–1823.

Schott, F., and L. A. Mysak, 1980: On the structure of low-frequency current fluctuations in the Strait of Georgia, *Atmos.-Ocean*, **18**, 181–194.

Wang, D. P., 1975: Coastal-trapped waves in a baroclinic ocean. *J. Phys. Oceanogr.*, **5**, 326–333.

Wilson, A. H., 1928: A generalized spheroidal wave equation. *Proc. Roy. Soc.*, A **118**, 617–635.

Yao, T., S. Pond and L. A. Mysak, 1982: Low-frequency subsurface current and density fluctuations in the Strait of Georgia. *Atmos.-Ocean*, **20**, 340–356.